Disease phenotype of a ferret *CFTR*-knockout model of cystic fibrosis

Xingshen Sun,[1] Hongshu Sui,[1] John T. Fisher,[1] Ziying Yan,[1,2] Xiaoming Liu,[1,2] Hyung-Ju Cho,[3] Nam Soo Joo,[3] Yulong Zhang,[1,2] Weihong Zhou,[1] Yaling Yi,[1] Joann M. Kinyon,[4] Diana C. Lei-Butters,[1] Michelle A. Griffin,[5] Paul Naumann,[5] Meihui Luo,[1] Jill Ascher,[6] Kai Wang,[7] Timothy Frana,[4] Jeffrey J. Wine,[3] David K. Meyerholz,[2,5] and John F. Engelhardt[1,2,8]

[1]Department of Anatomy and Cell Biology and [2]Center for Gene Therapy, Carver College of Medicine, University of Iowa, Iowa City, Iowa, USA. [3]Department of Psychology, Stanford University, Stanford, California, USA. [4]Department of Veterinary Diagnostic & Production Animal Medicine, College of Veterinary Medicine, Iowa State University, Ames, Iowa, USA. [5]Department of Pathology, Carver College of Medicine, University of Iowa, Iowa City, Iowa, USA. [6]Marshall Farms Group Ltd., North Rose, New York, USA. [7]Department of Biostatistics, College of Public Health, and [8]Department of Internal Medicine, Carver College of Medicine, University of Iowa, Iowa City, Iowa, USA.

Cystic fibrosis (CF) is a recessive disease that affects multiple organs. It is caused by mutations in CFTR. Animal modeling of this disease has been challenging, with species- and strain-specific differences in organ biology and CFTR function influencing the emergence of disease pathology. Here, we report the phenotype of a *CFTR*-knockout ferret model of CF. Neonatal *CFTR*-knockout ferrets demonstrated many of the characteristics of human CF disease, including defective airway chloride transport and submucosal gland fluid secretion; variably penetrant meconium ileus (MI); pancreatic, liver, and vas deferens disease; and a predisposition to lung infection in the early postnatal period. Severe malabsorption by the gastrointestinal (GI) tract was the primary cause of death in *CFTR*-knockout kits that escaped MI. Elevated liver function tests in *CFTR*-knockout kits were corrected by oral administration of ursodeoxycholic acid, and the addition of an oral proton-pump inhibitor improved weight gain and survival. To overcome the limitations imposed by the severe intestinal phenotype, we cloned 4 gut-corrected transgenic *CFTR*-knockout kits that expressed ferret *CFTR* specifically in the intestine. One clone passed feces normally and demonstrated no detectable ferret CFTR expression in the lung or liver. The animals described in this study are likely to be useful tools for dissecting CF disease pathogenesis and developing treatments.

Introduction

Cystic fibrosis (CF) is the most common life-threatening autosomal recessive condition among people of mixed European descent, with approximately 1 in 3,500 newborns affected each year. CF is caused by mutations in an epithelial chloride channel encoded by the *CFTR* gene (1–3). Tissues affected in CF include the lung, pancreas, liver, intestine, gallbladder, sweat gland, and male reproductive tract (2, 3). Phenotypic variability in the severity of disease in these tissues can be influenced by modifier genes, the type of *CFTR* mutation, and the environment in ways that are only partially understood (3, 4). CF mice have been an invaluable system for dissecting the biology of CFTR function and for demonstrating that genetic background can significantly influence CF-related phenotypes in this species (5, 6). Recently, the description of the neonatal CF pig phenotype has expanded the potential for modeling CF disease (7). Interestingly, CF mice and pigs develop either less or more severe disease in certain organ systems than do humans with CF, a fact that highlights species-specific differences in organ physiology and CFTR function. Additional CF models may help understanding of how the pleiotropic functions of CFTR in multiple organs influence the progression of lung disease — the most life-threatening aspect of CF being chronic bacterial infections of the airways.

The domestic ferret (*Mustela putorius furo)* is a potentially attractive species for modeling CF for 2 major reasons: its lung anatomy and lung cell biology are similar to those in humans, and it reproduces rapidly (42-day gestation and 4–6 months to sexual maturity). With regard to lung anatomy and lung cell biology, it is important to note that ferrets and humans have submucosal glands throughout their cartilaginous airways, whereas mice possess these glands only in the proximal trachea (8, 9). Submucosal glands express abundant CFTR in the serous tubules, which facilitate fluid and mucous secretion into the airway (10, 11); given that these structures are thought to play an important role in protecting the airways from bacterial infection (11, 12), their distribution may be important for modeling CF disease. Additionally, the goblet cell is the predominant secretory cell type of the human and ferret proximal cartilaginous airways, whereas the Clara cell is the analogous secretory cell type in mice (9, 13). Although Clara cells are also present in humans and ferret airways, they are limited to the bronchioles rather than being distributed throughout the proximal and distal airways as in mice (13, 14). For these reasons, we recently developed ferrets heterozygous for a *CFTR* exon 10 deletion, using adeno-associated virus gene targeting in fibroblasts, coupled with somatic cell nuclear transfer (SCNT) (15). Here, we report the neonatal disease phenotype in *CFTR*-null ferrets.

CFTR-knockout neonatal ferrets developed many of the pathologies observed in humans with CF, including meconium ileus (MI), pancreatic disease, liver disease, severely impaired nutrition, and a predisposition to lung infections during the early postnatal period. Liver disease in CF ferrets, as evident by a rise in liver function tests (LFTs) during the early postnatal period, was treatable by bile acid replacement. Additionally, improved nutritional status in the ferret model of CF could be achieved by administering an oral proton-

Conflict of interest: Jill Ascher is employed by Marshall Farms Group Ltd. as a veterinarian. Marshall Farms Group Ltd. will be distributing the animal model described in this manuscript.

Citation for this article: *J Clin Invest.* 2010;120(9):3149–3160. doi:10.1172/JCI43052.

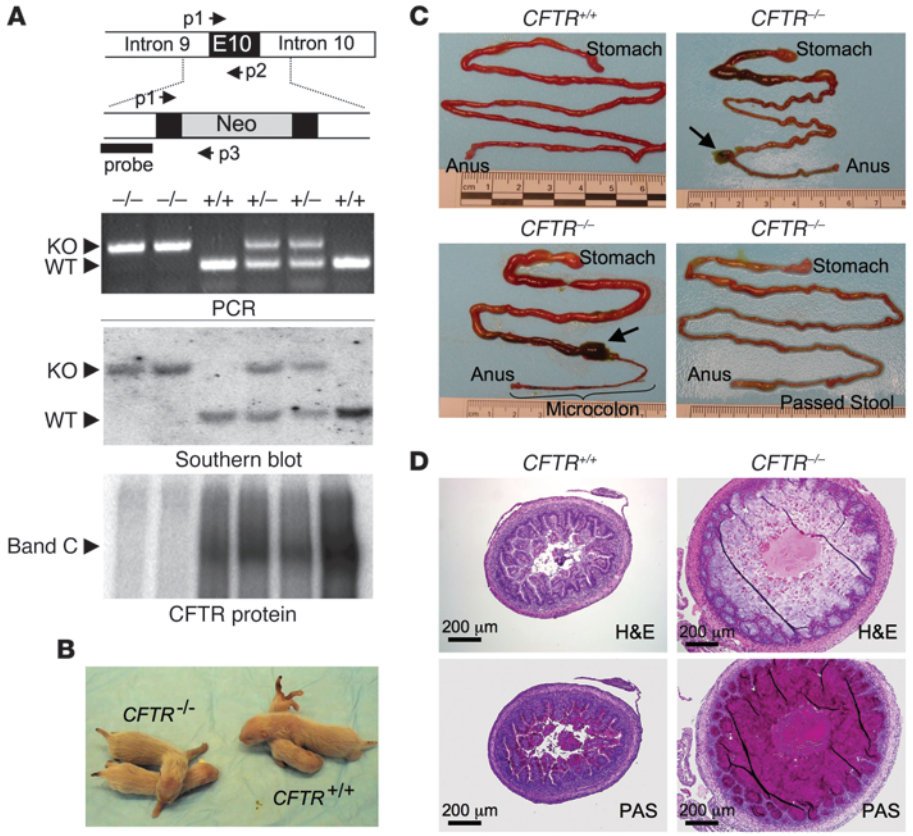

Figure 1

A subset of *CFTR*$^{-/-}$ kits are born with MI. (**A**) The schematic diagram of the targeted neomycin gene insertion into *CFTR* exon 10 (E10) outlines the approach used to generate the model and indicates the locations of primers and probes used for genotyping. The results of PCR and Southern blot genotyping for a litter of 6 kits, with the genotypes indicated, are shown. The bottom panel depicts the detection of CFTR protein from the intestine by CFTR immunoprecipitation, followed by in vitro phosphorylation in the presence of [γ-^{32}P]ATP and protein kinase A. The fully glycosylated band-C form of CFTR is shown. (**B**) Four kits at birth, with genotype indicated. (**C**) Intestines from kits at 36–48 hours after birth, with genotype indicated, demonstrating the variability in occurrence of MI and microcolon. Arrows mark perforations in the intestine caused by MI. (**D**) Histological analysis of the distal ileum/colon in H&E- or periodic acid-Schiff–stained (PAS-stained) sections for a *CFTR*$^{+/+}$ kit and *CFTR*$^{-/-}$ kit suffering from MI. All kits with MI demonstrated similar histopathology, with enhanced mucous production (i.e., enhanced periodic acid-Schiff staining in purple). Those *CFTR*$^{-/-}$ kits without MI demonstrated histology similar to that in the control animals (data not shown). Scale bar: 200 μm.

pump inhibitor. Because the frequency of MI in both the new CF pig and ferret models significantly limits their use, we corrected the gut defect by generating a transgenic *CFTR*-knockout ferret that expresses a HA-tagged C*FTR* cDNA under control of the intestinal-specific fatty acid–binding protein (*FABP*i) promoter. These studies led to the generation of a gut-corrected *CFTR*-knockout model that lacks MI at birth, in which expression of HA-tagged C*FTR* was observed in the intestine but not in the lung or liver. Although the adult CF ferret lung phenotype remains under investigation, these studies suggest that these new ferret models of CF may be of significant use for studying CF pathogenesis and developing treatments for CF.

Results

CFTR-knockout kits exhibit MI of variable penetrance. Eight heterozygous founder clones (*CFTR*$^{+/-}$) were expanded through a single generation of breeding, and their F1 *CFTR*$^{+/-}$ offspring gave rise to 313 kits containing 65 *CFTR*$^{+/+}$, 171 *CFTR*$^{+/-}$, and 77 *CFTR*$^{-/-}$ animals (Figure 1A). This ratio was not significantly different from the expected 1:2:1 inheritance of a recessive trait and indicates that prenatal lethality is not a consequence of deleting the *CFTR* gene in ferrets. Intestinal tissue from *CFTR*$^{-/-}$ kits expressed no CFTR protein as compared with that of *CFTR*$^{+/+}$ and *CFTR*$^{+/-}$ kits (Figure 1A). Within the first 24 hours of life, *CFTR*$^{-/-}$ kits were indistinguishable from *CFTR*$^{+/+}$ or *CFTR*$^{+/-}$ littermates, in terms of activity and weight (Figure 1B and Supplemental Figure 1; supplemental material available online with this article; doi:10.1172/JCI43052DS1). However, by 36 hours after birth, all *CFTR*$^{-/-}$ kits failed to thrive, and by 48 hours they were typically euthanized due to severe morbidity. Gross and histological pathologies indicated that the majority of kits (~75%) suffered from MI and failed to pass stool during the neonatal period (Figure 1C). Approximately half of the kits with MI died from intestinal perforation at the level of the ileum or colon (Figure 1C, arrows). Additionally, microcolon was observed in approximately 30% of the animals born with MI (Figure 1C). Interestingly, approximately 25% of newborn *CFTR*$^{-/-}$ kits passed meconium but nevertheless failed to thrive and died within 2–4 days after birth (Figure 1C). GI obstruction in *CFTR*$^{-/-}$ kits suffering from MI was associated with intestinal luminal mucus and mucous cell hyperplasia (Figure 1D). The occurrence of MI in ferret *CFTR*$^{-/-}$ kits (~75%) was greater than that for CF infants (~15%) (2, 16) and less than that seen in *CFTR*$^{-/-}$ pigs (100%) (7). Although CF mice do not present with classical MI at birth, they do suffer from gut obstruction at weaning, and this can significantly impair survival. Interestingly, the penetrance of gut obstruction in CF mice can vary significantly (0%–95% survival at weaning) depending on the background strain (5, 6), suggesting that genetic modifier genes significantly influence this phenotype in the mouse.

Analysis of the frequency of MI within the CF ferret colony suggested genetic influences for the development of severe intestinal complications at birth in *CFTR*$^{-/-}$ kits. Nine F2 generation male *CFTR*$^{+/-}$ hobs used for breeding gave rise to litters with MI frequencies ranging from 50%–100% (Table 1). Pearson's χ^2 test and Fisher's exact test for association demonstrated a statistically significant dependence of the variable MI frequency in CF offspring on the *CFTR*$^{+/-}$ hobs used for breeding ($P < 0.047$ for both tests). Additionally, a logistic regression was run in which the response variable was the MI status of the offspring and the explanatory variable was the hob identification. This analysis also suggested that inheritance of the MI phenotype was influenced by the hob ($P < 0.042$). Inclusion

Table 1
Frequency of MI in *CFTR*$^{-/-}$ kits born to 9 *CFTR*$^{+/-}$ hobs

Hob ID	910078S	910288S	910448S	910468S	910518S	910538S	910598S	910608S	910618S
CFTR$^{-/-}$ kits with MI	3	11	3	10	12	14	11	6	12
CFTR$^{-/-}$ kits without MI	3	1	3	0	2	1	4	0	5
Total kits born to hob	6	12	6	10	14	15	15	6	17
MI (%)	50%	92%	50%	100%	86%	93%	73%	100%	71%

Data were derived from 56 litters born from 40 jills bred randomly with 9 hobs.

of the female parents (i.e., jills) as an explanatory variable did not reach significance in this logistic regression, since the number of CF kits born to each of the 40 jills used in this analysis was too small, and only 8 of the jills were bred twice. These findings suggest that hereditary factors influence the occurrence of MI in *CFTR*$^{-/-}$ kits.

CFTR-knockout kits exhibit pancreatic lesions similar to those seen in CF infants but no overt histopathology of the liver or gallbladder. The newborn *CFTR*$^{-/-}$ pancreas was indistinguishable from that of *CFTR*$^{+/+}$ and *CFTR*$^{+/-}$ kits at the gross level, but histologic lesions were evident in all animals. Most, but not all, *CFTR*$^{-/-}$ acini and ductules were dilated with inspissated, eosinophilic zymogen secretions (Figure 2A). Microscopic changes in the pancreas are seen in approximately 75% of CF infants, with the majority of these cases (~72%) demonstrating histopathology similar to that seen in newborn *CFTR*$^{-/-}$ ferrets and a small minority of cases (~3%) demonstrating more severe lesions, with evidence of loss of exocrine tissue and the development of fibrosis (16, 17). Thus, the level of histopathology in the newborn *CFTR*$^{-/-}$ ferret pancreas appears to be quite similar to that seen in CF infants and significantly less severe than the extensive destruction observed in the exocrine pancreas of newborn CF pigs (7).

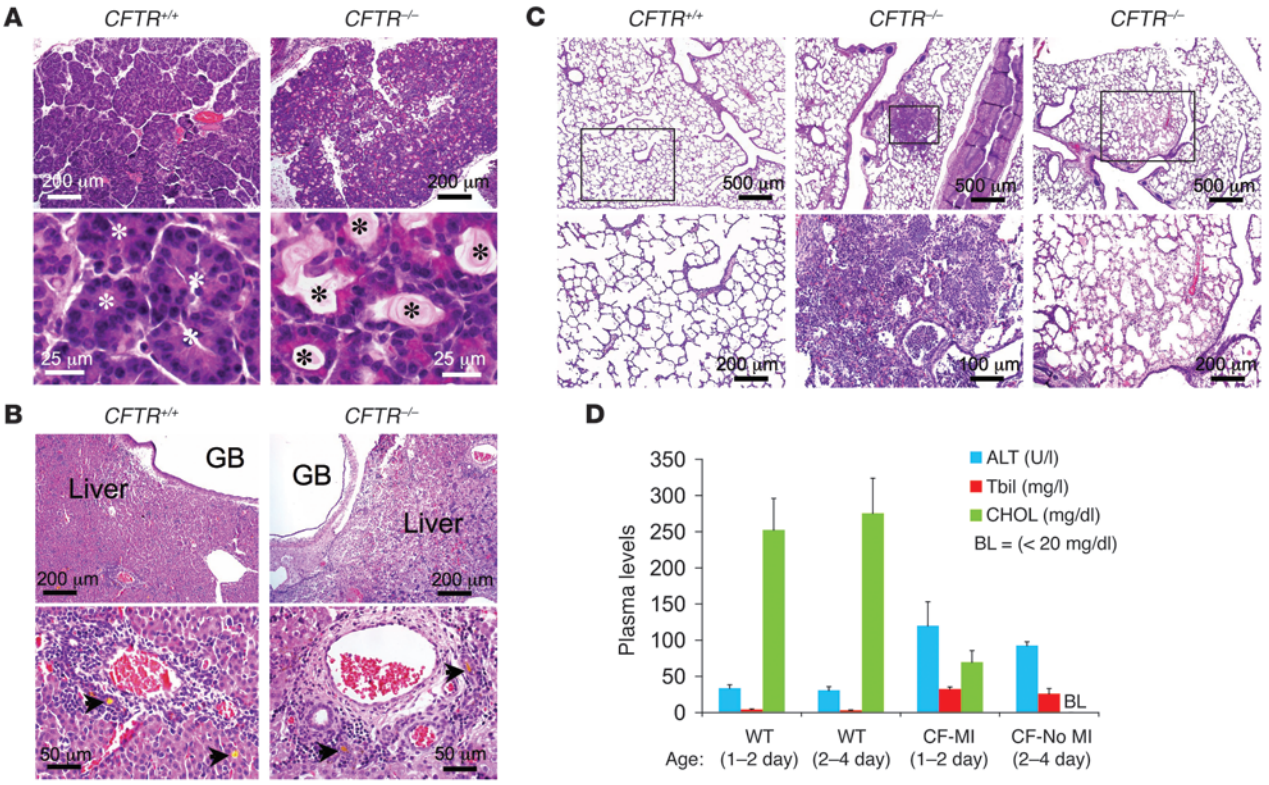

Figure 2
Primary organ pathologies observed in newborn *CFTR*$^{-/-}$ kits. (**A**) H&E-stained sections of the pancreas. Eosinophilic zymogen material filled exocrine acini (asterisks) of the *CFTR*$^{-/-}$ pancreas. (**B**) H&E-stained sections of the liver and gall bladder (GB). Arrowheads mark the bile-filled canaliculi infrequently seen in all genotypes. (**C**) H&E-stained section of the lung demonstrating the type of lung lesions observed in *CFTR*$^{-/-}$ newborn kits. The *CFTR*$^{-/-}$ examples are from the same animal that passed stool in Figure 1C and died at 48 hours. Boxed regions are enlarged in the bottom row and demonstrate evidence of fibrin deposition, necrosis, bacteria, and/or inflammation. (**D**) Blood chemistries for ALT, total bilirubin (Tbil), and cholesterol (CHOL) in animals of the indicated genotypes (WT, *CFTR*$^{+/+}$ and *CFTR*$^{+/-}$; CF, *CFTR*$^{-/-}$). CF kits were divided into 2 groups with and without MI. BL, below limits of detection. Blood was drawn at the time of euthanasia. Values depict the mean ± SEM (n = 5–9 animals in each group) (see Supplemental Figure 3 for additional blood chemistry data). Scale bar: 200 μm (**A**, top row, **B**, top row, and **C**, bottom left and right panels); 25 μm (**A**, bottom row); 50 μm (**B**, bottom row); 500 μm (**C**, top row); 100 μm (**C**, bottom center panel).

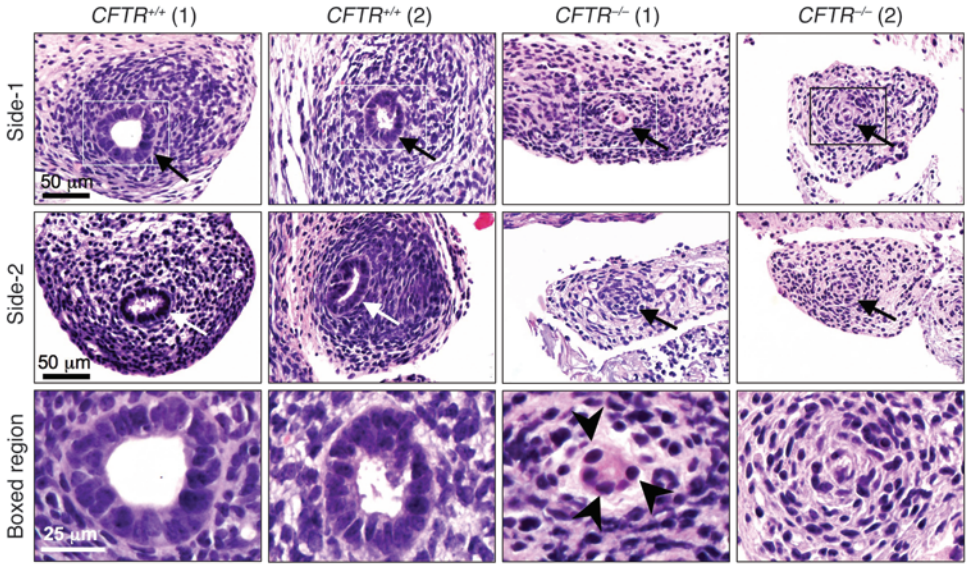

Figure 3

CFTR-knockout kits have a degenerate or absent vas deferens at birth. Panels depict H&E-stained sections of the vas deferens from 2 $CFTR^{+/+}$ and 2 $CFTR^{-/-}$ newborn kits. H&E-stained sections of both vasa deferentia from each animal are shown in the top 2 rows. The bottom row shows enlarged photomicrographs for the boxed regions in the top panels. Arrows in the top 2 rows mark the vas deferens in wild-type animals or the location of the absent or degenerate vas deferens in CF animals. The vas deferens of $CFTR^{-/-}$ animal 1 was degenerate on side-1 and absent on side-2, while $CFTR^{-/-}$ animal 2 demonstrated complete bilateral absence of the vas. Arrowheads mark remnant vas deferens epithelial cells in the enlarged image for $CFTR^{-/-}$ animal 1. See Supplemental Figure 2 for more $CFTR^{-/-}$ examples of vas deferens morphology. Scale bar: 50 μm (top and middle rows); 25 μm (bottom row).

The liver and gallbladder of newborn $CFTR^{-/-}$ kits were indistinguishable from those of $CFTR^{+/+}$ or $CFTR^{+/-}$ littermates at the gross and histological levels (Figure 2B).

CFTR-knockout kits have a degenerate or absent vas deferens at birth. Nearly all male adults with CF suffer from infertility caused by bilateral absence of the vas deferens (18). Most males with CF have an intact vas deferens at birth; however, mucoid obstruction of the vas deferens has been noted in newborns with CF, and unilateral absence of the vas deferens has been detected as early as 2 years of age (17). These findings have led to the prominent hypothesis that obstruction of the vas deferens and/or altered secretions lead to progressive degeneration in patients with CF (19). Histopathologic examination of the vas deferens in newborn $CFTR^{+/+}$, $CFTR^{+/-}$, and $CFTR^{-/-}$ littermates demonstrated considerable pathology in the newborn CF kits. Of the 5 $CFTR^{-/-}$ kits evaluated, the vas deferens was completely absent in about 50% of the spermatic cords (Figure 3). In the remainder the vas deferens was segmentally absent, with remnant epithelium characterized as small and degenerate to tortuous and serpentine (Supplemental Figure 2). In 1 out of the 5 $CFTR^{-/-}$ kits, there was complete bilateral absence of the vas deferens, while a normal vas deferens was consistently detected in all of the 5 control $CFTR^{+/+}$ and $CFTR^{+/-}$ kits.

Newborn CFTR-knockout kits that escape MI fail to thrive and exhibit early lung infections and elevated LFTs. Histopathologic analysis failed to ascertain the reason for early neonatal death of the 25% of $CFTR^{-/-}$ kits that passed meconium. Although the intestine appeared histologically normal in these animals, we noted evidence of bronchopulmonary pneumonia and aspiration (Figure 2C), which suggested that perhaps $CFTR^{-/-}$ kits were predisposed to aspiration-induced secondary infections. Blood chemistries in this subset of animals revealed that both plasma alanine aminotransferase (ALT) and bilirubin were consistently elevated while cholesterol levels were reduced (Figure 2D and Supplemental Figure 3); these findings suggested the potential for liver disease. Although clinically apparent liver disease in 1- to 5-year-old patients with CF is low (0.3%) (20), 53% of infants with CF demonstrate abnormally elevated LFTs, a feature that typically resolves itself by 2–3 years of age (21). Interestingly, these neonatal elevations in the levels of serum liver enzymes such as ALT were not associated with neonatal cholestasis when liver biopsies were evaluated (21). Such findings are similar to those seen in newborn $CFTR^{-/-}$ kits, which demonstrated no histopathologic lesions in the liver despite elevated LFTs (Figure 2B).

The reason for elevated LFTs in the majority of children with CF without histological signs of cholestasis remains unclear (21). However, children with CF frequently exhibit bile acid malabsorption by the intestine, which leads to altered enterohepatic circulation and hepatobiliary composition of bile acids (22–24). Excessive fecal bile acid loss has been proposed to influence fat and cholesterol absorption by the gut, bacterial flora in the gut, and the progression of liver disease through alterations in bile acid pool composition (24). Bile acids are synthesized from cholesterol by hepatocytes and transported into bile ducts in a conjugated form (25). Our findings of reduced serum cholesterol levels in 2- to 4-day-old $CFTR^{-/-}$ kits that escaped MI are consistent with impaired bile acid absorption by the gut and the depletion of cholesterol pools through defective fat absorption by the gut. Oral administration of the hydrophilic dihydroxylated bile acid ursodeoxycholic acid (UDCA) has been shown to normalize LFTs (including serum ALT and bilirubin levels) and to improve the nutritional status in patients with CF (26, 27).

For these reasons, we tested whether oral UDCA therapy of $CFTR^{-/-}$ kits might normalize liver function and improve nutrition. Additionally, $CFTR^{-/-}$ kits were gavaged with Golytely within the first 12 hours to enhance rapid meconium clearance and treated with antibiotics to prevent secondary lung infection during the early neonatal period. Among 20 $CFTR^{-/-}$ kits treated in this manner, 16 died of MI and 4 survived for 5–9 days but failed to gain weight (Figure 4A). Gross necropsy demonstrated that although there was no intestinal obstruction in the $CFTR^{-/-}$ kits, fat stores throughout the animals were depleted, consistent with sustained malnutrition (Figure 4B and Supplemental Figure 4C). UDCA treatment normalized serum ALT and bilirubin levels, as is the case in CF infants (27), but failed to normalize serum cholesterol levels, which remained low in comparison with treated controls (Figure 4C).

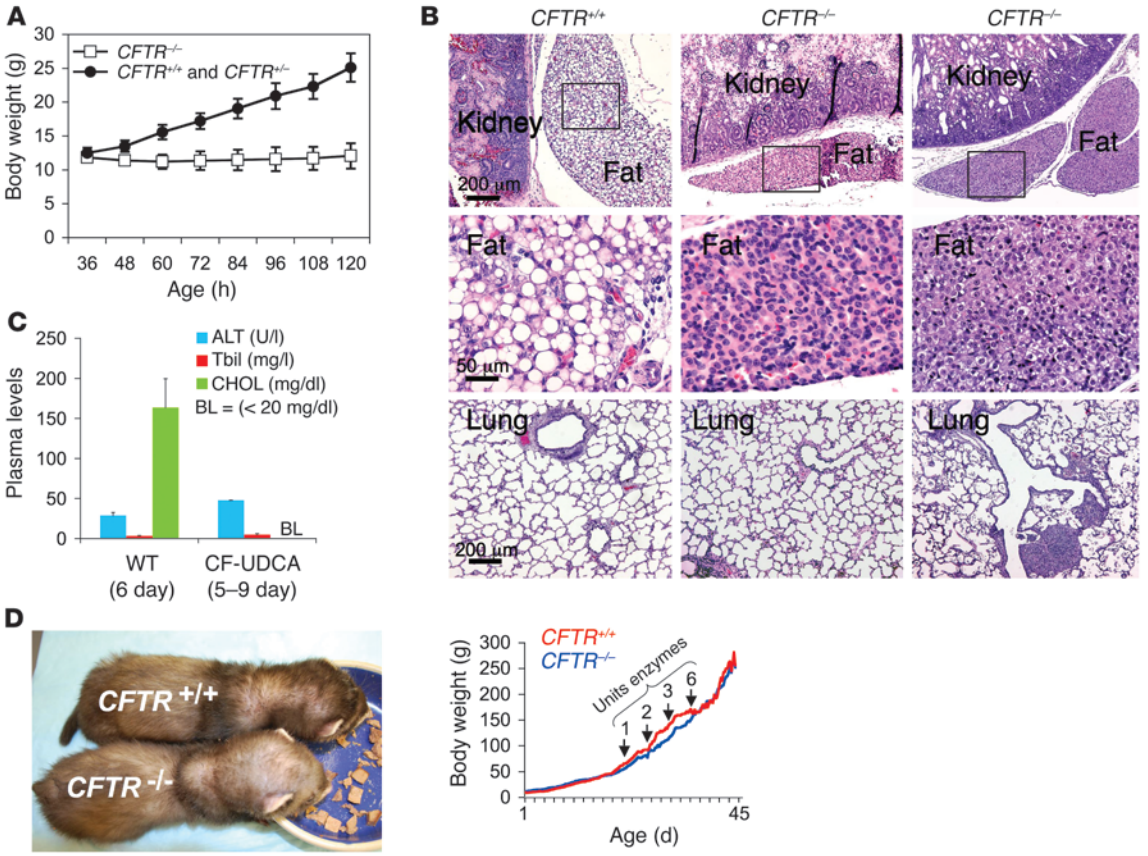

Figure 4

UDCA treatment lowers plasma ALT levels but does not enhance weight gain. (**A**) Weight gain of *CFTR*$^{+/+}$ and *CFTR*$^{+/-}$ kits (n = 4) and littermate *CFTR*$^{-/-}$ kits that passed stool and did not have MI (n = 4). One of the *CFTR*$^{-/-}$ kits survived to 9.5 days but failed to gain weight after the time points shown. Data depict the mean ± SEM. (**B**) H&E-stained sections of the kidney and perirenal adipose tissue and lung from 5- to 9-day-old kits. Adipocytes demonstrate depletion of fat stores (fewer white spaces) in both *CFTR*$^{-/-}$ kits. Three of the four *CFTR*$^{-/-}$ kits treated with UDCA demonstrated lung lesions similar to that shown in the right panel of the bottom row (also see Supplemental Figure 4). The middle row shows enlarged images for the boxed regions in the top panels. Scale bar: 200 μm (top and bottom rows); 50 μm (middle row). (**C**) Blood chemistries for UDCA-treated kits (WT, *CFTR*$^{+/+}$ and *CFTR*$^{+/-}$; CF, *CFTR*$^{-/-}$). Blood was drawn at the time of euthanasia. Values represent the mean ± SEM (n = 3–4 animals in each group). (**D**) *CFTR*$^{-/-}$ and *CFTR*$^{+/+}$ kits treated with UDCA and omeprazole. The left panel demonstrates size at 45 days of age, and the right panel depicts weight gain. The timing of oral pancreatic enzyme replacement is shown by the arrows, with the lipase units administered with each feeding marked above each arrow.

Three out of the four *CFTR*$^{-/-}$ kits developed respiratory distress and showed signs of multifocal bronchopneumonia — with the lungs demonstrating intralesional neutrophils, macrophages, hemorrhage, fibrin, and bacterial colonies (Figure 4B and Supplemental Figure 4). Airways and alveoli were patent and showed no evidence of inflammation, hemorrhage, or bacterial colonization in control-treated *CFTR*$^{+/+}$ and *CFTR*$^{+/-}$ kits. Although control lungs were free of pathology, it is currently unclear whether lung lesions in the *CFTR*$^{-/-}$ kit were due to the inability of the weakened animals (i.e., nutritionally compromised) to eradicate the bacteria associated with aspirated material. In a small subset of *CFTR*$^{-/-}$ kits (n = 3) that passed meconium, we also attempted pancreatic enzyme replacement, but this failed to improve either the nutritional status or the survival of these animals.

Oral administration of a proton-pump inhibitor improves nutrition in the CFTR-knockout model. Bile acids play an important role in intestinal lipid digestion and absorption, cholesterol homeostasis, and excretion of lipid-soluble xenobiotics (25). The solubilization and reabsorption of bile acids by the gut can also be influenced by fecal pH (28). Given that gut pH would likely be reduced in the context of CF, due to impaired pancreatic secretion of bicarbonate, we reasoned that raising the gut pH by oral administration of the proton-pump blocker omeprazole might allow for better bile acid–mediated absorption of fat in the gut and thereby improve the nutritional status of CF kits. Omeprazole has been used to enhance the function of pancreatic enzyme supplementation in CF patients with residual steatorrhea to improve fat absorption (29). Indeed, oral administration of UDCA and an omeprazole-containing liquid elemental diet led to significantly improved weight gain in a *CFTR*$^{-/-}$ kit during the first 16 days of treatment; weight gain was comparable to that of a *CFTR*$^{+/+}$ littermate control that was treated identically. However, at 16 days the weight gain of the *CFTR*$^{-/-}$ kit began to slow in comparison to that of the control, and thus the animals were supplemented with oral pancreatic enzymes. After several weeks of increasing enzyme intake, the *CFTR*$^{-/-}$ kit recovered enough weight to nearly match

Table 2
Weight gain of *CFTR*$^{-/-}$ kits reared on UDCA and omeprazole

Genotype (experiment)	Birth weight in g	Peak weight in g (age [d])	Weight at death/euthanasia in g (age [d])	Apparent cause of death
+/– (1)	9.7	901 (180)	901 (180)[A]	Alive
–/– (1)	11.3	1,194 (165)	1,033 (180)[A]	Alive
+/+ (2)	8.6	88.7 (19)	89.2 (20)	—
–/– (2)	8.9	31.9 (19)	29.8 (20)	Acute aspiration (rare neutrophils)
+/+ (3)	8.6	168.2 (29)	157.1 (32)	—
–/– (3)	8.4	76.9 (27)	71.7 (32)	Rectal prolapse
+/+ (4)	9.1	41.7 (10)	62.1 (13)	—
–/– (4)	9.0	14.9 (10)	14.2 (13)	Unknown (focus of pneumonia noted)
+/– (5)	10.4	28.9 (7)	28.9 (7)	—
–/– (5)	10.1	11.8 (6)	10.2 (7)	Unknown (intestinal obstruction noted)

[A]Animals were healthy at the time this most recent weight was taken.

that of the control kit (Figure 4D). Four additional *CFTR*$^{-/-}$ kits have been reared using this same approach and also had improved weight gain during the neonatal period; although in these 4 cases, weight gain was only approximately 25%–50% of that of controls (Table 2). One of these *CFTR*$^{-/-}$ kits died acutely at 20 days, due to a massive aspiration while nursing. The second *CFTR*$^{-/-}$ kit died at 32 days, due to a rectal prolapse. The third and fourth *CFTR*$^{-/-}$ kits died at 7 and 13 days of age. The cause of death was undetermined in the 7-day-old kit, but it did have a small focus of pneumonia; the 13-day-old kit had intestinal obstruction noted during pathology examination. Histopathologic examination of these animals demonstrated increased pancreatic inflammation and loss of exocrine tissue consistent with progression of CF disease. In addition, localized atelectasis was not uncommon and complete obstruction of airways was at times detected (Supplemental Figures 5 and 6).

Bacteriology of bronchioalveolar lavage fluid and fecal samples. Despite improved weight gain in treated *CFTR*$^{-/-}$ kits that lack MI, approximately half still died within the first week of life. To evaluate the types of bacteria found in the lungs of these and other *CFTR*$^{-/-}$ kits that died within the first month of life, we performed bacteriologies on bronchioalveolar lavage (BAL) fluid. To control for the type of bacteria deposited in the lung due to gut obstruction, we also evaluated *CFTR*$^{-/-}$ kits that died from MI (Table 3). As anticipated, those animals that succumbed to MI had a much higher abundance of enteric bacterial flora in their lungs. By contrast, 2 additional species (*Staphylococcus* and *Streptococcus)* were found in the BAL of 2-day-old *CFTR*$^{-/-}$ kits without MI at higher abundance in comparison with that of wild-type and heterozygous controls (Table 3 and Supplemental Figure 7). In *CFTR*$^{-/-}$ kits that died after the first week of life, the density of bacteria in the lung was similar to or only slightly greater than that of controls animals. In the oldest *CFTR*$^{-/-}$ animal that died at 32 days, *Streptococcus spp, alpha haemolytic* was the only species found in the BAL, and this differed from those found in the control. We also evaluated the types of bacteria found in feces from the oldest surviving *CFTR*$^{-/-}$ and littermate control ferrets; however, no obvious differences were found (Table 3).

Tracheas from CFTR-knockout ferrets demonstrate defects in cAMP-induced chloride permeability and submucosal gland secretions. Lung disease is the most life-threatening aspect of CF (2, 3). Defective CFTR-mediated anion transport and enhanced fluid absorption by the surface airway epithelium is thought to hinder bacterial clearance (3). Additionally, submucosal glands of the cartilaginous airways express abundant CFTR and have been proposed to play an important role in the pathogenesis of CF lung disease, as a consequence of defective secretion of antibacterial factor containing fluid into the airway lumen (3, 11, 30). Although the natural progression of lung disease in adult *CFTR*$^{-/-}$ ferrets remains to be delineated, functional studies on newborn *CFTR*$^{-/-}$ ferret tracheas demonstrate that this model features abnormalities characteristic of the proximal airways of CF patients, including defective cAMP-induced chloride permeability and submucosal gland fluid secretion (Figure 5). Using transepithelial potential difference (TEPD) measurements in an ex vivo tracheal xenograft model, we found that *CFTR*$^{-/-}$ tracheas lack cAMP-dependent changes in Cl^- permeability (Figure 5, A and B), a feature that is characteristic of TEPD defects seen in the nasal epithelium of human patients with CF (3). No significant difference was observed in amiloride-sensitive TEPD among the various genotypes; although this finding differs from those of studies of the human CF nasal epithelium that demonstrate elevated amiloride-sensitive changes in TEPD in comparison with non-CF (3), it is consistent with findings from human CF and non-CF tracheal xenografts (31), and thus may be a consequence of functional differences in the region (i.e., nose vs. trachea) of airway epithelium evaluated or a specific feature of the xenograft model. Fluid secretion from submucosal glands of *CFTR*$^{-/-}$ tracheas was also significantly reduced — secretion in response to 3 μM forskolin was reduced by 7.4 fold and secretion in response to 1 μM carbachol was reduced by half (Figure 5, C and D, and Supplemental Figure 8). Glandular secretory responses in human CF proximal airways show this same pattern — a large reduction in response to cAMP agonists and a smaller reduction in response to Ca^{2+} agonists (11, 30). There was no significant difference between CF and non-CF ferret tracheal xenografts, in terms of the glandular area relative to the unit length of the surface airway epithelium ($P = 0.679$), demonstrating that the observed differences in secretion were not due to altered gland size between genotypes.

A gut-corrected transgenic CFTR-knockout ferret model corrects MI at birth. Similar to the situation for the CF pig and mouse models, the severity of intestinal complications in the *CFTR*$^{-/-}$ ferret model significantly hinders its application as a research model. In CF mice, correction of intestinal complications by expressing the human *CFTR* cDNA under the direction of the *FABP*i promoter has proven invaluable (32). Taking advantage of this approach, we generated a transgene cassette that expresses the C*FTR* cDNA under the direction of the *FABP*i promoter (Figure 6A). This *CFTR* cDNA contains a HA-tag inserted into the fourth extracellular

Table 3
Bacteriology of BAL and fecal samples

Animal (experiment)	CFTR genotype	Age (d)	Sample	Density of growth[A]	Organism
1 (1)	+/+	2	BAL	+	*Streptococcus spp,* alpha haemolytic
2 (1)	+/+	2	BAL	-	No growth
3 (1)	+/+	2	BAL	+	*Actinomyces spp*
4 (1)	–/–	2	BAL	++++	*Staphylococcus spp*; *Enterococcus spp*
5 (1)	–/– (MI)[B]	2	BAL	++	*Enterococcus spp*
6 (1)	–/– (MI)	2	BAL	++++	*Bacillus spp*
7 (2)	+/–	2	BAL	+	*Corynebacterium spp.*; *Enterococcus spp.*; *Actinomyces spp*
8 (2)	+/+	2	BAL	+	*Streptococcus spp*, alpha haemolytic; *Enterococcus faecalis*; *Proteus mirabilis*
9 (2)	–/– (MI)	2	BAL	++++	*Enterococcus faecalis*; *Coagulase negative Staph group*; *Corynebacterium spp*; *Chryseobacterium indologenes*; *Clostridium perfringens*
10 (2)	–/–	2	BAL	++++	*Streptococcus spp*, alpha haemolytic; *Enterococcus species*; *Enterococcus faecalis*; *Staphylococcus epidermidis*; *Staph pseudintermedius*; *Proteus mirabilis*
11 (3)	+/–	7	BAL	+	*Staph pseudintermedius*; *Streptococcus spp*, alpha haemolytic
12 (3)	–/–	7	BAL	++	*Streptococcus spp*, alpha haemolytic; *Coag negative Staph group*; *Clostridium perfringens*; *Proteus mirabilis*
13 (4)	+/+	20	BAL	++	*Staph pseudintermedius*; *Streptococcus spp*, alpha haemolytic
14 (4)	–/–	20	BAL	++	*Enterococcus faecalis*; *Staph pseudintermedius*
15 (5)	+/+	32	BAL[C]	+	*Coagulase negative Staph group*; *Non-fermenter species*; *Haemophilus spp*
16 (5)	–/–	32	BAL[C]	+	*Streptococcus spp*, alpha haemolytic
17 (6–8)	+/–	174[D]; 176[E]; 178[F]	Feces	++++	*Proteus vulgaris*[D]; *Proteus mirabilis*[E,F]; *Streptococcus spp*, alpha haemolytic[E,F]; *E. coli*[D,E,F]; *Enterococcus faecalis*[D,E,F]; *Enterococcus faecium*[F]; *Clostridium perfringens*[D,E]; *Corynebacterium spp*[F]
18 (6–8)	–/–	174[D]; 176[E]; 178[F]	Feces	++++	*Proteus mirabilis*[D,E,F]; *Streptococcus spp*, alpha haemolytic[D,E,F]; *E. coli*[D,E,F]; *Enterococcus faecalis*[D,E]; *Enterococcus spp.*[F]; *Enterococcus faecium*[F]; *Clostridium perfringens*[D,E,F]

[A]Evaluation of growth was based on bacterial colonies appearing in quadrants 1 (+), 2 (++), 3 (+++), 4 (++++) of the nonselective bacterial cultures plates. [B]Animals that died from MI are denoted by "(MI)." All other *CFTR*$^{-/-}$ animals passed stool. [C]Single lobe lavages were used to retain integrity of histopathology. Letters D, E, and F indicate a correlation between the day in age of collection and the presence of the bacteria found on that day. Feces were collected every other day for a total of 3 collections.

loop and demonstrated normal chloride channel function in vitro (data not shown). The linear fragment of the FABPi-HA-C*FTR*-PGK-*Zeo* cassette was transfected into primary fibroblasts derived from a female *CFTR*$^{-/-}$ 28-day-old embryo, and selected pools of the transgenic cells were used for SCNT. Four transgenic FABPi-HA-C*FTR*/*CFTR*$^{-/-}$ clones were born harboring the transgene cassette in their genomic DNA (Figure 6C), but only 1 survived the early postnatal period and passed stool normally (clone-1). The 3 additional clones born had to be euthanized within 36 hours after birth due to MI (Figure 6B, clone-2, -3, and -4). The surviving clone-1 was also euthanized to determine the expression patterns of recombinant CFTR, and this clone had a grossly normal intestine, lacking any signs of MI (Figure 6B, clone-1). Analysis of intestinal CFTR expression in the 4 clones demonstrated that clone-1 expressed the highest levels of CFTR protein (Figure 6D), correlating with the lack of a neonatal MI phenotype in this clone. Additionally, primary fibroblasts, liver, and lung were harvested from clone-1 to confirm tissue-specific expression of CFTR prior to nuclear transfer recloning and expansion of the line. Results from this analysis demonstrated that FABPi-HA-C*FTR*/*CFTR*$^{-/-}$ clone-1 expressed CFTR in the intestine but not in the lung and liver (Figure 6E). Endogenous CFTR protein was expressed in all of these organs from *CFTR*$^{+/+}$ kits but not *CFTR*$^{-/-}$ kits (Figure 6E). Currently, SCNT is being performed to expand the clone-1 line.

Discussion

Although the gene responsible for CF was discovered more than 2 decades ago, it still remains unclear how CFTR defects lead to the airway disease that is responsible for most CF deaths. Such slow progress can be attributed to the lack of an adequate animal model of CF airway disease. Although CF mice have illuminated so many aspects of CF pathophysiology, they do not display a human-like CF airways disease. The need for different animal models of CF prompted the creation of CF pig and ferret models. We believe this is the first report of early phenotypic features in a genetically engineered ferret model of CF, demonstrating that it shares many of the abnormalities seen in newborn humans with CF. To our knowledge, CF is the first human disease for which directed engineering has generated 2 non-rodent knockout models, and comparative studies on organ-specific CF disease phenotypes in 4 species (human, mouse, ferret, and pig) will greatly expand our understanding of CF pathogenesis.

The greatest cause of CF neonatal mortality in all species is intestinal obstruction, but with important differences in penetrance, age at onset, and phenotype. Human with CF and CF pigs and ferrets display a true MI at birth, whereas CF mice develop intestinal complications at a different stage in development (i.e., weaning to solid chow). The penetrance of MI varies greatly among humans with CF (~15%), CF ferrets (~75%), and CF pigs (100%), and a wide

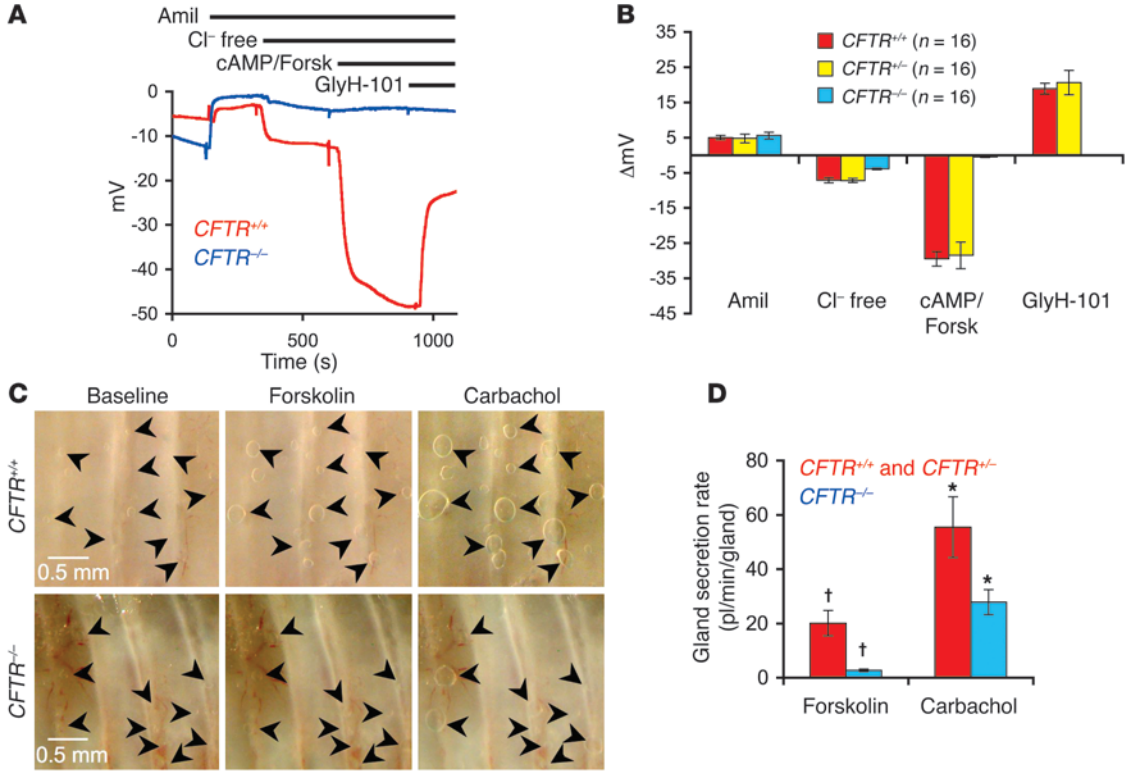

Figure 5

Airway defects observed in *CFTR*$^{-/-}$ kits. (**A** and **B**) TEPD measurements in tracheal xenografts generated from *CFTR*$^{+/+}$, *CFTR*$^{+/-}$, and *CFTR*$^{-/-}$ kits. (**A**) Representative tracings of TEPD following sequential addition of the following drugs to the lumen of the airway xenografts: 100 μM amiloride (Amil), Cl^--free buffer, 10 μM forskolin/200 μM 8-ctp-cAMP (cAMP/Forsk), and 100 μM GlyH-101. (**B**) The cumulative data for transepithelial voltage responses (ΔVt) to the various buffer changes is shown for the indicated genotypes. Results depict the mean ± SEM transepithelial voltage responses for N measurements in 4 independent xenografts for each genotype (TEPD was evaluated 4 times for each xenograft on different days). (**C** and **D**) Analysis of submucosal gland secretion in tracheal xenografts from *CFTR*$^{+/+}$, *CFTR*$^{+/-}$, and *CFTR*$^{-/-}$ kits. (**C**) Representative en face photomicrographs of glandular secretory droplets are shown (several marked by arrows) at baseline (unstimulated), in response to 30-minute stimulation with 3 μM forskolin, and in response to 30-minute stimulation with 1 μM carbachol. Scale bar: 0.5 mm. (**D**) Averaged data for glandular secretory rates in response to 3 μM forskolin or 1 μM carbachol for the indicated genotypes. Results depict mean ± SEM (n = 10 *CFTR*$^{+/+}$ and *CFTR*$^{+/-}$ xenografts and n = 13 *CFTR*$^{-/-}$ xenografts). $^{\dagger}P < 0.05$; $^{*}P < 0.05$, using the Student's t test. Typically 10–15 glands were measured for each xenograft sample. The average rate of secretion for all glands in a given sample was used to calculate the mean ± SEM. The total number of glands analyzed was 110 for *CFTR*$^{+/+}$ and *CFTR*$^{+/-}$ xenografts and 151 for *CFTR*$^{-/-}$ xenografts.

variance in intestinal obstruction is also observed in CF mice (0%–100%) depending on the strain background (5, 6). Modifier genes appear to influence the occurrence of MI in infants with CF based on monozygous and dizygous CF twin/triplet studies (33), and our studies also suggest that the hob exerts a genetic influence for development of MI in *CFTR*$^{-/-}$ ferrets. Complete penetrance of MI in the *CFTR*$^{-/-}$ piglets studied to date may be a consequence of their intestinal anatomy and/or their inbred status.

The severity of CF pancreatic pathology at birth differs widely across the species, with pigs being most severe (7), ferrets and humans being similar (16, 17), and mice being least severe (6). The sparing of the pancreas in newborn mice has been attributed to alternative Ca^+-activated chloride channels in this organ (34), and it will be interesting to determine whether this single factor can account for the variation across all 4 species. The vas deferens is another tissue that demonstrates variable CF disease pathology between the species. Congenital bilateral absence of the vas deferens is diagnosed in nearly all (~99%) of adult males with CF (18). Even though "congenital absence" implies that this structure is not present at birth, most infant males with CF have an intact vas deferens at birth (17), and increased detection rate in younger patients suggests that disease in this tissue is a degenerative process that may begin prior to birth in some individuals and culminate with destruction by adulthood (19). Interestingly, with the exception of the CF ferret that demonstrates an absent or degenerate vas deferens at birth, other CF animal models have not replicated this phenomenon — CF mice have minor histologic changes to the vas deferens but are fertile (35), and CF pigs appear to have intact vas deferens at birth (7). Whether CF pigs will develop disease of the vas deferens in adulthood remains to be determined.

Of all species, CF newborn ferrets have the most severely impaired nutritional status at birth. The ferret intestinal tract is unique in comparison with those of humans, pigs, and mice. As an obligate carnivore, ferrets lack a cecum, which is found in humans, pigs, and mice; this structure is known to assist in the digestion of plant material. The ferret also has a shorter intestinal transit time in comparison to other species (36, 37). These features likely impose special nutrient requirements, which to date remain to be defined

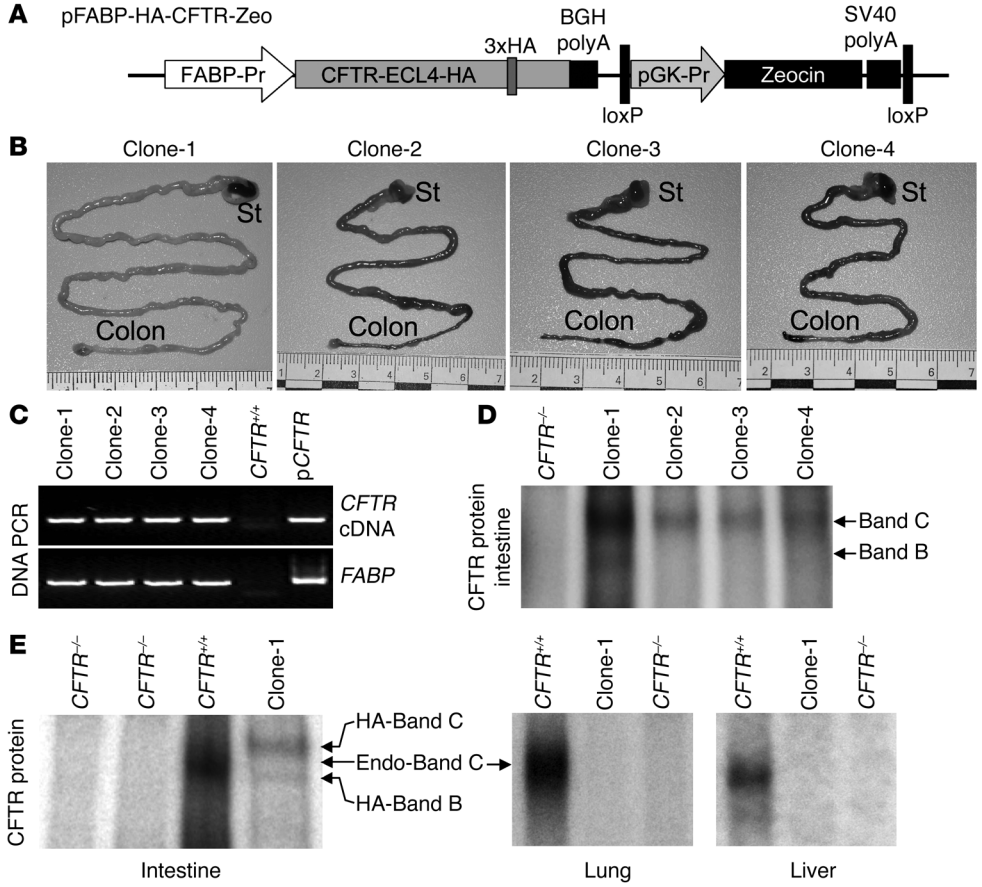

Figure 6

Generation of a gut-corrected transgenic *CFTR*$^{-/-}$ ferret by SCNT. (**A**) Schematic diagram of the FAPBi-HA-C*FTR*-PGK-*Zeocin* cassette used to generate transgenic ferrets expressing HA-tagged CFTR under the control of the FABPi promoter (FABP-Pr) and bovine growth hormone (BGH) poly-A. pFABP, plasmid FABP. (**B**) Primary fibroblasts were transfected with the linear transgenic fragment shown in **A**, and selected pools were used for SCNT. Four cloned kits were born, and the gross morphology of the intestine is shown. Clone-1 passed stool normally within 24 hours of birth, while clone-2, -3, and -4 suffered from MI and failed to pass stool. St, stomach. (**C**) PCR genotyping of the 4 transgenic FABP-HA-C*FTR*/*CFTR*$^{-/-}$ cloned kits. Genomic DNA from a *CFTR*$^{+/+}$ kit served as a negative control, while plasmid DNA (pCFTR) harboring the transgene cassette was used as a positive control. The PCR reactions were designed to specifically detect a segment of the HA-tag and C*FTR* cDNA or the rat *FABP*i promoter as shown. (**D**) Detection of CFTR protein levels in intestinal lysates from the 4 FABP-HA-C*FTR*/*CFTR*$^{-/-}$ clones and a *CFTR*$^{-/-}$ kit by CFTR immunoprecipitation, followed by in vitro phosphorylation in the presence of [γ-^{32}P]ATP and protein kinase A. (**E**) Comparison of CFTR protein levels using in vitro phosphorylation of immunoprecipitated CFTR from the intestine, lung, and liver of FABP-HA-C*FTR*/*CFTR*$^{-/-}$ clone-1. Lanes show results for *CFTR*$^{+/+}$, *CFTR*$^{-/-}$, and FABP-HA-C*FTR*/*CFTR*$^{-/-}$ clone-1 kits. The fully glycosylated band-C and partially processed band-B forms of CFTR are shown (note that migration of transgenic CFTR is slightly slower than that of endogenous CFTR, due to the presence of the HA-tag).

at the molecular level. The complete lack of weight gain in newborn CF ferrets suggests that intestinal CFTR plays a critical role in nutritional absorption in this species. Additionally, the pancreatic pathology and bile acid–dependent liver abnormalities observed at birth in CF ferrets may also play a role in their poor nutrition.

Oral administration of a proton-pump inhibitor significantly improved nutrition in CF ferrets, suggesting that CFTR-dependent perturbations in GI pH may have a significant impact on the absorption of fat and/or other key nutrients in this species. Proton-pump inhibitors have been extensively used in CF patients suffering from sustained steatorrhea while on pancreatic enzymes, and these drugs appear to improve nutritional status according to some reports (29, 38). Furthermore, reduced GI pH in a *Cftr*$^{-/-}$ mouse model has been suggested to impair lipolysis and fat absorption by the intestine (wild type, 94% ± 0.3% absorption vs. knockout, 89.7% ± 1.2% absorption), despite normal lipase and bicarbonate secretion by the pancreas (39), and this defect was corrected by oral administration of a proton-pump inhibitor. Interestingly, elevated bile salt secretion into the feces was also observed in *Cftr*$^{-/-}$ mice, despite normal levels of bile salt secretion by the biliary system (39). The authors of this study concluded that *Cftr*$^{-/-}$ mice suffer from fat malabsorption due to impairment of the duodenal bicarbonate production that is required for efficient lipolysis and uptake of fatty acids (39). It is interesting, however, that ΔF508-CFTR mice do not suffer from the same lipolysis and fatty acid uptake defects seen in *Cftr*$^{-/-}$ mice (39). Although further studies on intestinal biology in the ferret are needed to understand how CFTR in this organ might directly influence lipid absorption in this species, it seems plausible that *CFTR*$^{-/-}$ ferrets suffer from a relatively pronounced intestinal pH imbalance that influences fat absorption in a similar manner as in *Cftr*$^{-/-}$ mice. These and other issues will likely be clarified by the production of a gut-corrected *CFTR*$^{-/-}$ ferret model.

Understanding how CFTR malfunction contributes to the extreme GI phenotypes in these CF animal models should help to improve management of the more subtle pathologies seen in humans with CF. However, a major impetus to controlling or genetically eliminating the GI pathology is to allow the models to grow to maturity so that the natural progression of lung disease can be determined. Thus far, we know that the basic defects in airway bioelectric and submucosal gland secretory properties reproduce those seen in human CF. Furthermore, rearing *CFTR*$^{-/-}$ kits under protocols that improved nutrition did not completely prevent early fatal lung infections that were also seen in nutritional compromised animals. Despite improved nutrition, neonatal *CFTR*$^{-/-}$ kits had increased bacterial counts and isolates from BAL fluid that subsided after the first week. After the

first week, lung infections did not appear to be the primary cause of death in *CFTR*$^{-/-}$ kits. It is interesting to speculate that neonatal aspiration events may serve as inoculation mechanisms, and defective bacterial eradication compromises the ability of the CF lung to clear normal early pathogens like control animals. Although the number of animals analyzed remains low, our observations of early fatal lung infections and rectal prolapse in *CFTR*$^{-/-}$ kits is also similar to clinical observations in CF infants during the early 1950s (40). In this case study of 68 CF infants, over 60% died before the age of 1 year, while only 15% survived 2–13 years. More than half of the CF infants who contracted lung infection at birth died (excluding those with MI), and failure to thrive during the neonatal period despite a ravenous appetite was common. These observations are quite similar to our findings with *CFTR*$^{-/-}$ kits. As with humans, the improved use of broad-spectrum antibiotics during the neonatal period may help to improve survival in this ferret model of CF. These initial findings in the lung and other organs of *CFTR*$^{-/-}$ ferrets, suggest that the ferret may be a useful model for dissecting CF pathophysiology and developing therapies. This report also describes the production of what we believe to be the first transgenic ferret using SCNT, and such methods will expand opportunities for genetically dissecting CF pathogenesis in the ferret model.

Methods

Animals and genotyping. All animal experimentation was performed according to protocols approved by the Institutional Animal Care and Use Committees of the University of Iowa. Eight *CFTR*$^{+/-}$ (F0) male ferret clones of sable coat color background were used to expand the colony by breeding to wild-type sable coat color jills. F1 *CFTR*$^{+/-}$ male (hob) and female (jill) offspring from different litters were then crossed to generate F2 litters composed of *CFTR*$^{+/+}$, *CFTR*$^{+/-}$, and *CFTR*$^{-/-}$ offspring. Genotyping of F1 ferrets was performed by Southern blotting, using blood drawn at 5 weeks of age and methods as previously described (15). In brief, 10 μg genomic DNA was digested with *Afl*II and Southern blotted with an intron-9 α-^{32}P-labeled probe (15). A 2.8-kb fragment represents the wild-type CFTR allele, and a 4.5-kb fragment represents the mutant CFTR allele. A rapid PCR method for genotyping tail clips was developed for F2 offspring as follows: a small piece of tail tissue (0.3 to 0.5 cm in length) was lysed in 500 μl lysis buffer (10 mM Tris, pH 8.0, 100 mM NaCl, 1 mM EDTA, 0.5% SDS, and 100 μg/ml Proteinase K) at 55°C for 4 hours. After phenol-chloroform extraction, DNA was precipitated with isopropanol and then rehydrated in 10 mM Tris, pH 8.0, buffer. The DNA concentration was adjusted to 0.1 μg/μl, and 1 μl (100 ng DNA) was used in each PCR reaction with 1 μl primer mix and 23 μl AccuPrime Pfx Supermix (Invitrogen). PCR conditions were 95°C for 5 minutes, followed by 30 cycles of 95°C for 15 seconds, 55°C for 15 seconds, and 68°C for 15 seconds. Primer p1 (TGATGATTATGGGAGAGTTGGAGCC) and primer p2 (TTGATGGTGCCAGGCATGATCC) are complementary to sites upstream and downstream of the target insertion site in exon 10 of the ferret *CFTR* gene. Amplification using the above-described PCR conditions generated a 100-bp DNA fragment from only the wild-type CFTR allele; the 1.9-kb product from the targeted allele was too long to be amplified. The targeted allele was amplified using a third primer p3 (TGGCGGCCGTTACTAGTGGAT), which is complementary to the sequence within the PGK-Neomycin cassette. The p1/p3 primer set amplified a 180-bp product. Primers p1, p2, and p3 were mixed together at a final concentration of 25 pM/μl for each primer and used in the above-described PCR reaction. PCR products (100 bp and 180 bp) were resolved on a 1.5% agarose gel.

CFTR immunoprecipitation and phosphorylation assays. Intestine, liver, and lung from newborn ferret kit were harvested, flushed with saline in the case of the intestine, and snap frozen in liquid nitrogen. This tissue was pulverized and lysed on ice in RIPA buffer (150 mM NaCl, 20 mM Tris-HCl, 1% Triton X-100, 0.1% SDS, 0.5% deoxycholate, pH 8.0) containing a protease inhibitor cocktail (Roche) for 30 minutes. The samples were vortexed every 10 minutes during the lysis procedure. The insoluble fraction was then removed by centrifugation (16,100 *g*, 4°C, 10 minutes). Equal amounts (1 mg) of soluble protein were diluted in 1 ml RIPA buffer containing 0.1% Tween 20 and then precleared (3 times) using an irrelevant mouse IgG1 antibody linked to protein G DynaBeads (Invitrogen). This preclearing was necessary to prevent bead aggregation during the immunoprecipitation. The soluble protein was immunoprecipitated using a combined cocktail of mouse anti-CFTR antibodies, M3A7 and MM13-4 (both from Chemicon) and anti-HA antibody (Roche), and in vitro phosphorylated as previously described (41). The samples were then resolved on 7.5% SDS-PAGE gels, fixed, dried, exposed to a phosphoscreen, and scanned with a Typhoon 8600 Variable Mode Imager (Molecular Dynamics).

Bioelectric measurement in tracheal xenografts. Functional assessment of TEPD was evaluated in *CFTR*$^{+/+}$, *CFTR*$^{+/-}$, and *CFTR*$^{-/-}$ tracheal xenografts. The xenograft approach involves cannulating tracheas from newborn kits with flexible tubing, followed by subcutaneous transplantation into *nu/nu* mice (31). Xenografts were irrigated twice weekly with F12 medium and remained air filled. In this model, the transplanted airways vascularize by 2–3 weeks and are fully differentiated by 5–6 weeks following transplantation. TEPDs were measured using two 1 M KCl/5% agar electrodes linked to a voltmeter through a set of calomel electrodes within a 1 M KCl solution. The positive agar electrode was placed in the luminal tubing of one end of the xenograft, and the negative electrode was placed subcutaneously in the back of the mouse. Xenografts were first irrigated with HEPES phosphate-buffered Ringers solution (HPBR-D) (10 mM HEPES, pH. 7.4, 145 mM NaCl, 5 mM KCl, 1.2 mM $MgSO_4$, 1.2 mM Ca-gluconate, 2.4 mM K_2HPO_4, 0.4 mM KH_2PO_4, and 100 μM 4,4′-diisothiocyanostilbene-2,2′-disulfonic acid), followed by irrigation with the following buffers after sequential changes: (a) HPBR-D plus 100 μM amiloride, (b) chloride-free HPBR-D (with gluconate replacing Cl^-) plus 100 μM amiloride, (c) buffer b plus 200 μM 8-ctp-cAMP and 10 μM forskolin, and (d) buffer c plus 50 μM $CFTR_{inh}$-GlyH101. Millivolt recordings were taken by means of a computer-assisted recorder.

Functional measurement of gland secretions in tracheal xenografts. Rates of mucous secretion from single submucosal glands were determined on excised *CFTR*$^{+/+}$, *CFTR*$^{+/-}$, and *CFTR*$^{-/-}$ tracheal xenografts, as previously described (42), with modification to optimize xenograft viability. Xenografts were harvested, placed in minimal essential medium with antibiotics, and shipped overnight at 4°C from the University of Iowa to Stanford University. Tracheal xenografts were open along the posterior trachealis muscle, and dissected tracheal segments were mounted mucosal side up in a chamber, without removing the cartilage, at 4°C. The tissue surface was blotted dry and then further dried with a gentle stream of 95% O_2/5% CO_2 gas, followed by application of water-saturated mineral oil to the surface. The bath temperature was then gradually increased to minimize potential gland secretions caused by a sudden temperature change. During functional measurement, the tracheal segments were maintained in 37°C Krebs-Ringer bicarbonate buffer (KRB), bubbled with 95% O_2/5% CO_2 in a humidified atmosphere. The composition of the KRB was 115 mM NaCl, 2.4 mM K_2HPO_4, 0.4 mM KH_2PO_4, 25 mM $NaHCO_3$, 1.2 mM $MgCl_2$, 1.2 mM $CaCl_2$, 10 mM glucose, and 1.0 μM indomethacin (pH 7.4). Following measurements of baseline secretory rates for 20 minutes, 3 stimulatory conditions were tested sequentially for 30 minutes with the following solutions: (a) serosal (bath) application of 3 μM forskolin alone, (b) serosal application of 3 μM forskolin and 100 nM carbachol, and (c) serosal application of 1 μM carbachol alone. Only the gland secretory rates for stimulatory conditions a and c are presented in the results. The genotype-dependent

trends for stimulatory condition b were intermediate to conditions a and c. Condition b was tested to evaluate the synergy of cAMP- and Ca^{2+}-dependent pathways for glandular secretion that have previously been described (43). Digital images of the spherical mucous bubbles under mineral oil were obtained at 5-minute intervals, based on which the secretory rates for individual glands were calculated using ImageJ software (http://rsbweb.nih.gov/ij/). Typically, approximately 10–15 glands were imaged per xenograft tissue sample. The average number of gland bubbles observed per mm^2 was 1.8 ± 0.7 for non-CF samples and 1.9 ± 0.3 for CF samples. To confirm that differences in glandular secretory rates between CF and non-CF xenografts were not due to differences in gland size, we performed morphometric analysis on the samples analyzed. After functional assays were completed, the xenograft tissue was fixed in formalin and paraffin embedded, and 5–6 sections at approximately 500-μm intervals through the depth of the trachea were obtained. The unit length of the surface airway basal lamina and the glandular area were measured for each section using Metamorph software. The total length of the surface airway epithelium (basal lamina) was then divided by the glandular area for each sample to produce a glandular size index for each sample. On average, approximately 75 photomicrographs were evaluated for each xenograft sample (n = 5 for non-CF and n = 6 for CF). Statistical comparison of the glandular size indexes using the Student's t test demonstrated that the glandular size did not differ significantly between the 2 genotypes.

Neonatal clinical care of $CFTR^{-/-}$ kits. Two treatment protocols were developed to enhance postnatal survival and reduce the risk of intestinal obstruction caused by MI. Both protocols included administering metronidazole (5 mg/kg in 100 μl dextrose saline, s.c.) 4 times daily beginning at the time of birth, starving the animals for the first 3 hours after birth, and then administering a 150- to 200-μl Golytely gavage (Braintree Laboratories Inc.) using a fire-polished microloader pipette tip (Eppendorf Inc.) (see Supplemental Figure 9 for example of gavage tube components). The gavage was repeated every 6 hours, up to 3 times, until meconium was passed. After the CF kits passed meconium, they were fed 150–200 μl Elecare (Abbott Laboratories) supplemented with UDCA (5 mg/kg) and/or omeprazole (5 mg/kg) 4 times daily by gavage. When the diet was supplemented with pancreatic enzymes, Viokase-V was used and dosed according to lipase units as specified in the legend for Figure 4. Once genotypes were known, typically at 12 to 18 hours after birth, the litter size was reduced, such that only the $CFTR^{-/-}$ kits and an equal number of controls ($CFTR^{+/+}$ and/or $CFTR^{+/-}$) were kept. When kits were weaned at 5 weeks of age, they were fed a slurry of Elecare hydrated solid chow (Marshall Farms) twice daily, mixed with 1 lipase unit of Viokase-V per 10 grams of body weight (the amount of food eaten with each feeding was recorded for these calculations).

Blood chemistries. Blood chemistries were performed using a VetScan VS2 (Abaxis), using blood drawn at the time of clinical death and necropsy. Mammalian Liver Profile rotors from Abaxis were used to assess plasma levels of alkaline phosphatase, ALT, bile acids, total bilirubin, total cholesterol, gamma glutamyl transferase, and blood urea nitrogen. Total and direct bilirubin levels in the plasma were measured using 2 kits from Diazyme Inc. for total bilirubin (DZ150A-K) and direct bilirubin (DZ151A-K); to find the level of indirect bilirubin in the plasma, we used the following formula: indirect bilirubin = total bilirubin – direct bilirubin.

Histopathology. Standard histopathology analysis was performed on paraffin sections from formalin-fixed tissues. Tissues were collected at the time of euthanasia (clinical death) and immediately placed in 10% neutral buffered formalin for at least 72 hours. Tissues were then paraffin embedded, sectioned (4–5 μm), and stained with H&E or periodic acid-Schiff. A modified Gram-Twort procedure was used to identify Gram-positive and Gram-negative bacteria in tissue sections (44). Briefly, this technique uses a Gram stain protocol, followed by application of Twort solution (containing nuclear fast red). This procedure results in Gram-positive bacteria staining blue/black and Gram-negative bacteria staining red/pink. Histopathological examination was performed by a veterinary pathologist, and age-matched $CFTR^{-/-}$ and $CFTR^{+/+}$ or $CFTR^{+/-}$ controls were used.

Bacteriology of BAL fluid and fecal samples. BAL was collected when animals were euthanized and performed in a laminar flow hood under sterile surgical conditions. A small incision was made to expose the trachea, and a 23-gauge angiocatheter was inserted into the proximal end of the trachea and stabilized using surgical sutures. Sterile saline (1–2 ml) was used to lavage the lung. This was repeated 3 times, and BAL fluid was pooled. Fecal samples were collected from the oldest $CFTR^{-/-}$ and control animal, and 0.2 grams were resuspended in 3 ml of sterile saline by vortexing with glass beads. Three percent of each BAL fluid or fecal sample was plated onto various types of bacterial growth media for bacteriologies. Fecal and BAL samples were streaked directly and were plated from enrichment broth onto selective and nonselective agar media (blood agar, anaerobic blood agar, MacConkey agar, colistin and nalidixic acid agar, anaerobic colistin and nalidixic acid reducible agar, chocolate agar [for BAL only], Hectoen enteric agar [for fecal only], brilliant green agar [for fecal only], XLT4 agar [for fecal only], tetrathionate broth, chopped meat glucose broth, brain heart infusion broth). Cultures were incubated aerobically and anaerobically for 24–48 hours at 35°C. All plates were examined for bacterial growth and visually assessed for bacterial types and quantity. Growth was measured semiquantitatively based on colony distribution on the plates within the 4-quadrant streak pattern. Growth on nonselective media was ranked for growth based on the occurrence of colonies in quadrants 1–4 (++++), 1–3 (+++), 1–2 (++), or 1 only (+). Representative colonies from mixed cultures were subcultured to purity onto appropriate media. Bacterial identification was based on colony morphology, gram stain, and biochemical reactions (45). Extended bacterial identification was performed if needed using an API 20E test kit.

SCNT cloning of a $CFTR^{-/-}$ transgenic ferret with intestine-specific expression of wild-type ferret CFTR. A transgene cassette containing the rat FABPi promoter (32) (gift of Jeffrey Whitsett, University of Cincinnati, Cincinnati, Ohio, USA) driving the expression of a HA-tagged CFTR cDNA with a bovine growth hormone poly-A was generated in plasmid pcDNA3.1. This cassette also contained a floxed PGK promoter-driven Zeocin/SV40–poly-A resistance gene cassette for selection of transfected cells. The wild-type CFTR cDNA was engineered to contain a 3xHA tag in extracellular loop 4 by PCR-mediated cloning, and its sequence was based on that previously described for generating 3xHA-tagged human CFTR (46). The cDNA sequence of the 3xHA-tag was 5′-agtactcagagcCTCGAGTACCCTTACGACGTTCCTGATTACGCTGCTAGCTACCCTTACGACGTTCCTGATTACGCTTACCCTTACGACGTTCCTGATTACGCTGCTTCTataaatagcagt-3′ (sequences in lowercase letters show homology to the junctional CFTR sequence, and those in uppercase letters represent the 3xHA-tag sequence). The amino acid sequence of this tag is as follows: *STQSL*E<u>YPYDVPDYAAS</u><u>YPYDVPDYAYPYDVPDYAAS</u>*INSS* (italicized amino acids are junctional CFTR amino acids, and non-italicized amino acids are the HA-tag sequence; the underlined letters are the 3 HA amino acid epitopes). The linear fragment encompassing the FABPi-HA-CFTR/PGK-Zeocin transgenic cassette was isolated by PmeI digestion of the pFABPi-HA-CFTR-Zeo plasmid, followed by agarose-gel purification. This gel-purified fragment was then transfected into primary fibroblasts generated from a female 28-day-old $CFTR^{-/-}$ kit. The transfected $CFTR^{-/-}$ fibroblasts were selected in 50 μg/ml Zeocin (Invitrogen) for 3 weeks, and the zeocin-resistant cells from this pool were used as donors for SCNT according to previously described protocols (15, 47). Cloned kits were evaluated for the presence of the transgene in their genomic DNA using PCR and phenotyped for MI and tissue expression of the HA-CFTR transgene.

Statistics. Statistical significance for all comparisons (with the exception of inheritance studies) was assessed using an unpaired, 2-tailed Student's *t* test. Inheritance of the MI phenotype was performed using the Pearson's χ^2 test, Fisher's exact test, and logistic regression. For logistic regression, the response variable was the MI status of the offspring, and the explanatory variable was the hob and/or jill identification. In all statistical analyses, *P* values of less than 0.05 were considered significant.

Acknowledgments

This work was supported by grants from the NHLBI (RC1HL099516), NIDDK (P30DK054759, R37DK047967), and the Cystic Fibrosis Foundation (ENGELH08XX0) as well as by the Roy J. Carver Chair in Molecular Medicine. We are extremely grateful for the clinical advice of Michael J. Goodheart, Kalpaj R. Parekh, Hubert Fornalik, Zoe Stewart, David Stoltz, Lynda Ostegaard, and Michael Welsh. We also thank Gergely Lukacs for providing the HA-tagged sequence inserted into the ECL4 domain of human HA-tagged CFTR. We also gratefully acknowledge Christine Blaumueller for editorial contributions.

Received for publication March 19, 2010, and accepted in revised form June 2, 2010.

Address correspondence to: John F. Engelhardt, Room 1-111 BSB, Department of Anatomy and Cell Biology, College of Medicine, University of Iowa, 51 Newton Road, Iowa City, Iowa 52242, USA. Phone: 319.335.7744; Fax: 319.335.6581; E-mail: john-engelhardt@uiowa.edu.

1. Riordan JR, et al. Identification of the cystic fibrosis gene: cloning and characterization of complementary DNA. *Science*. 1989;245(4922):1066–1073.
2. Welsh MJ, Ramsey BW, Accurso F, Cutting GR. *The Metabolic and Molecular Basis of Inherited Disease*. New York, New York, USA: McGraw-Hill; 2001.
3. Rowe SM, Miller S, Sorscher EJ. Cystic fibrosis. *N Engl J Med*. 2005;352(19):1992–2001.
4. Drumm ML, et al. Genetic modifiers of lung disease in cystic fibrosis. *N Engl J Med*. 2005;353(14):1443–1453.
5. Egan ME. How useful are cystic fibrosis mouse models? *Drug Discov Today Dis Models*. 2009; 6(2):35–41.
6. Guilbault C, Saeed Z, Downey GP, Radzioch D. Cystic fibrosis mouse models. *Am J Respir Cell Mol Biol*. 2007;36(1):1–7.
7. Rogers CS, et al. Disruption of the CFTR gene produces a model of cystic fibrosis in newborn pigs. *Science*. 2008;321(5897):1837–1841.
8. Choi HK, Finkbeiner WE, Widdicombe JH. A comparative study of mammalian tracheal mucous glands. *J Anat*. 2000;197(pt 3):361–372.
9. Robinson NP, Venning L, Kyle H, Widdicombe JG. Quantitation of the secretory cells of the ferret tracheobronchial tree. *J Anat*. 1986;145:173–188.
10. Engelhardt JF, et al. Submucosal glands are the predominant site of CFTR expression in the human bronchus. *Nat Genet*. 1992;2(3):240–248.
11. Wine JJ, Joo NS. Submucosal glands and airway defense. *Proc Am Thorac Soc*. 2004;1(1):47–53.
12. Dajani R, et al. Lysozyme secretion by submucosal glands protects the airway from bacterial infection. *Am J Respir Cell Mol Biol*. 2005;32(6):548–552.
13. Pack RJ, Al-Ugaily LH, Morris G, Widdicombe JG. The distribution and structure of cells in the tracheal epithelium of the mouse. *Cell Tissue Res*. 1980;208(1):65–84.
14. Plopper CG, Hill LH, Mariassy AT. Ultrastructure of the nonciliated bronchiolar epithelial (Clara) cell of mammalian lung. III. A study of man with comparison of 15 mammalian species. *Exp Lung Res*. 1980;1(2):171–180.
15. Sun X, et al. Adeno-associated virus-targeted disruption of the CFTR gene in cloned ferrets. *J Clin Invest*. 2008;118(4):1578–1583.
16. Oppenheimer EH, Esterly JR. Cystic fibrosis of the pancreas. Morphologic findings in infants with and without diagnostic pancreatic lesions. *Arch Pathol*. 1973;96(3):149–154.
17. Oppenheimer EH, Esterly JR. Pathology of cystic fibrosis review of the literature and comparison with 146 autopsied cases. *Perspect Pediatr Pathol*. 1975;2:241–278.
18. Jarzabek K, et al. Cystic fibrosis as a cause of infertility. *Reprod Biol*. 2004;4(2):119–129.
19. Gaillard DA, Carre-Pigeon F, Lallemand A. Normal vas deferens in fetuses with cystic fibrosis. *J Urol*. 1997;158(4):1549–1552.
20. Scott-Jupp R, Lama M, Tanner MS. Prevalence of liver disease in cystic fibrosis. *Arch Dis Child*. 1991;66(6):698–701.
21. Lindblad A, Glaumann H, Strandvik B. Natural history of liver disease in cystic fibrosis. *Hepatology*. 1999;30(5):1151–1158.
22. Harries JT, Muller DP, McCollum JP, Lipson A, Roma E, Norman AP. Intestinal bile salts in cystic fibrosis: studies in the patient and experimental animal. *Arch Dis Child*. 1979;54(1):19–24.
23. Weber AM, Roy CC, Morin CL, Lasalle R. Malabsorption of bile acids in children with cystic fibrosis. *N Engl J Med*. 1973;289(19):1001–1005.
24. Weber AM, Roy CC. Bile acid metabolism in children with cystic fibrosis. *Acta Paediatr Scand Suppl*. 1985;317:9–15.
25. Hofmann AF. Bile acids: trying to understand their chemistry and biology with the hope of helping patients. *Hepatology*. 2009;49(5):1403–1418.
26. Cotting J, Lentze MJ, Reichen J. Effects of ursodeoxycholic acid treatment on nutrition and liver function in patients with cystic fibrosis and longstanding cholestasis. *Gut*. 1990;31(8):918–921.
27. Scher H, Bishop WP, McCray PB Jr. Ursodeoxycholic acid improves cholestasis in infants with cystic fibrosis. *Ann Pharmacother*. 1997;31(9):1003–1005.
28. Hofmann AF, Mysels KJ. Bile acid solubility and precipitation in vitro and in vivo: the role of conjugation, pH, and Ca2+ ions. *J Lipid Res*. 1992; 33(5):617–626.
29. Proesmans M, De Boeck K. Omeprazole, a proton pump inhibitor, improves residual steatorrhoea in cystic fibrosis patients treated with high dose pancreatic enzymes. *Eur J Pediatr*. 2003;162(11):760–763.
30. Salinas D, et al. Submucosal gland dysfunction as a primary defect in cystic fibrosis. *FASEB J*. 2005;19(3):431–433.
31. Zhang Y, Yankaskas J, Wilson J, Engelhardt JF. In vivo analysis of fluid transport in cystic fibrosis airway epithelia of bronchial xenografts. *Am J Physiol*. 1996;270(5 pt 1):C1326–1335.
32. Zhou L, Dey CR, Wert SE, DuVall MD, Frizzell RA, Whitsett JA. Correction of lethal intestinal defect in a mouse model of cystic fibrosis by human CFTR. *Science*. 1994;266(5191):1705–1708.
33. Blackman SM, et al. Relative contribution of genetic and nongenetic modifiers to intestinal obstruction in cystic fibrosis. *Gastroenterology*. 2006;131(4):1030–1039.
34. Gray MA, Winpenny JP, Porteous DJ, Dorin JR, Argent BE. CFTR and calcium-activated chloride currents in pancreatic duct cells of a transgenic CF mouse. *Am J Physiol*. 1994;266(1 pt 1):C213–221.
35. Reynaert I, et al. Morphological changes in the vas deferens and expression of the cystic fibrosis transmembrane conductance regulator (CFTR) in control, deltaF508 and knock-out CFTR mice during postnatal life. *Mol Reprod Dev*. 2000;55(2):125–135.
36. Schwarz LA, Solano M, Manning A, Marini RP, Fox JG. The normal upper gastrointestinal examination in the ferret. *Vet Radiol Ultrasound*. 2003;44(2):165–172.
37. Bell JA. Ferret nutrition. *Vet Clin North Am Exot Anim Pract* 1999;2(1):169–192, viii.
38. Tran TM, Van den Neucker A, Hendriks JJ, Forget P, Forget PP. Effects of a proton-pump inhibitor in cystic fibrosis. *Acta Paediatr*. 1998;87(5):553–558.
39. Bijvelds MJ, Bronsveld I, Havinga R, Sinaasappel M, de Jonge HR, Verkade HJ. Fat absorption in cystic fibrosis mice is impeded by defective lipolysis and post-lipolytic events. *Am J Physiol Gastrointest Liver Physiol*. 2005;288(4):G646–653.
40. Bodian M, ed. *Fibrocystic Disease Of The Pancreas: A Congenital Disorder Of Mucus Production-mucosis*. New York, New York, USA: Grune & Stratton, Inc.; 1953.
41. Ostedgaard LS, et al. Processing and function of CFTR-DeltaF508 are species-dependent. *Proc Natl Acad Sci U S A*. 2007;104(39):15370–15375.
42. Joo NS, Wu JV, Krouse ME, Saenz Y, Wine JJ. Optical method for quantifying rates of mucus secretion from single submucosal glands. *Am J Physiol Lung Cell Mol Physiol*. 2001;281(2):L458–468.
43. Choi JY, et al. Synergistic airway gland mucus secretion in response to vasoactive intestinal peptide and carbachol is lost in cystic fibrosis. *J Clin Invest*. 2007;117(10):3118–3127.
44. Ollett WS. A method for straining both Gram-positive and Gram-negative bacteria in sections. *J Path Bact*. 1947;59(1-2):357–358.
45. Quinn PJ, Carter ME, Markey BK, Carter GR. *Clinical Veterinary Microbiology*. London, United Kingdom: Mosby Ltd; 1994.
46. Glozman R, Okiyoneda T, Mulvihill CM, Rini JM, Barriere H, Lukacs GL. N-glycans are direct determinants of CFTR folding and stability in secretory and endocytic membrane traffic. *J Cell Biol*. 2009;184(6):847–862.
47. Li Z, et al. Cloned ferrets produced by somatic cell nuclear transfer. *Dev Biol*. 2006;293(2):439–448.